



Experimental Investigation of a Thermochemical Reactor for High-Temperature Heat Storage via Carbonation-Calciation Based Cycles

Journal Article

Author(s):

Wild, Michael ; Lüönd, Lorenz; Steinfeld, Aldo 

Publication date:

2021-10-06

Permanent link:

<https://doi.org/10.3929/ethz-b-000508462>

Rights / license:

[Creative Commons Attribution 4.0 International](#)

Originally published in:

Frontiers in Energy Research 9, <https://doi.org/10.3389/fenrg.2021.748665>

Funding acknowledgement:

173438 - Continuous Solar-Driven Calcination of Borates Assisted with a Novel Combined Sensible-Heat/Thermochemical Storage (SNF)



Experimental Investigation of a Thermochemical Reactor for High-Temperature Heat Storage via Carbonation-Calcination Based Cycles

Michael Wild, Lorenz Lüönd and Aldo Steinfeld*

Department of Mechanical and Process Engineering, ETH Zurich, Zurich, Switzerland

OPEN ACCESS

Edited by:

Alicia Bayon,
Arizona State University, United States

Reviewed by:

Ernesto Mura,
Independent Researcher, Germany
Qiang Liu,
China University of Petroleum, China
Carlos Ortiz,
Loyola Andalusia University, Spain

*Correspondence:

Aldo Steinfeld
aldo.steinfeld@ethz.ch

Specialty section:

This article was submitted to
Process and Energy Systems
Engineering,
a section of the journal
Frontiers in Energy Research

Received: 30 July 2021

Accepted: 17 September 2021

Published: 06 October 2021

Citation:

Wild M, Lüönd L and Steinfeld A (2021)
Experimental Investigation of a
Thermochemical Reactor for High-
Temperature Heat Storage via
Carbonation-Calcination
Based Cycles.
Front. Energy Res. 9:748665.
doi: 10.3389/fenrg.2021.748665

We report on the design of a modular, high-temperature thermochemical energy storage system based on endothermic-exothermic reversible gas-solid reactions for application in concentrated solar power and industrial thermal processes. It consists of an array of tubular reactors, each containing an annular packed bed subjected to radial flow, and integrated in series with a thermocline-based sensible thermal energy storage. The calcination-carbonation of limestone, $\text{CaCO}_3 \leftrightarrow \text{CaO} + \text{CO}_2$, is selected as the reversible thermochemical reaction for the experimental demonstration. Synthesized 4.2 mm-mean size agglomerates and 2 mm-mean size granules of CaO with 42 %wt sintering-inhibitor MgO support attained reaction extents of up to 84.0% for agglomerates and 31.9% for granules, and good cycling stability in pressure-swing and temperature-swing thermogravimetric runs. A lab-scale reactor prototype is fabricated and tested with both formulations for 80 consecutive carbonation-calcination cycles at ambient pressure using a temperature-swing mode between 830°C and 930°C. The reactor exhibited stable cyclic operation and low pressure drop, and yielded specific gravimetric and volumetric heat storage capacities of 866 kJ/kg and 322 MJ/m³ for agglomerates, respectively, and 450 kJ/kg and 134 MJ/m³ for granules, respectively.

Keywords: thermochemical storage, solar, process heat, calcium looping, reactor

INTRODUCTION

Thermal Energy Storage (TES) enables the use of intermittent concentrated solar energy for supplying high-temperature heat round-the-clock to industrial processes and for solar thermal power generation (Glatzmaier, 2011; Henry et al., 2020). The main TES approaches are based on sensible, latent and thermochemical heat, and combinations thereof. Sensible heat storage has been mainly deployed as molten salt (Kuravi et al., 2013) and thermocline based systems (Mostafavi Tehrani et al., 2017; Zanganeh et al., 2012). The latter can be applied to store heat at temperatures

Abbreviations: χ , reaction extent [-]; FS, full-scale; HTF, heat transfer fluid; L, standard liters; MFM, mass flowmeters; MFC, mass flow controllers; SHS, sensible heat storage; TES, thermal energy storage; TCS, thermochemical heat storage; TGA, thermogravimetric analysis.

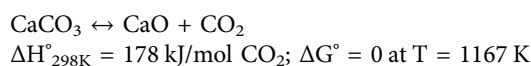
above 600°C using a packed-bed of rocks with a separate heat transfer fluid (HTF) (Hänchen et al., 2011; Zanganeh et al., 2012). However, thermocline-based concepts inherently suffer from a temperature profile degradation after multiple charging-discharging cycles, leading to an undesired drop in the HTF outflow temperature during discharge (Stekli et al., 2013). Several mitigation strategies have been explored, such as multi-tank arrangements (Roos and Haselbacher, 2021), flow flushing and extraction (Geissbühler et al., 2019), and combined sensible-latent heat storage systems (Zanganeh et al., 2015). In general, current technologies based on sensible and latent heat storage are limited in temperature by materials constraints and in energy storage density by their specific heat capacity and enthalpy of phase change.

Of special interest is the thermochemical heat storage, which makes use of reversible endothermic-exothermic reactions for storing high-temperature heat for long term and with superior energy storage density (Abedin and Rosen, 2011; André and Abanades, 2020; Carrillo et al., 2019; King et al., 2019; Mette et al., 2012; Peng et al., 2017; Yuan et al., 2018). Reactors for thermochemical heat storage using gas-solid reactions can be classified into directly and indirectly irradiated reactors. Directly irradiated reactor concepts use solids directly exposed to concentrated solar radiation, for example in granular flows (Schrader et al., 2020) and rotary kilns (Neises et al., 2012), providing efficient radiative heat transfer directly to the reaction site. In contrast, indirectly irradiated concepts use a separate HTF to transfer the heat into the solids, either by direct contact or via a heat exchanger. A widely applied example in this category are fixed bed reactors, which feature higher volumetric heat storage capacity than particle flows and avoid the complexity of moving particles at high temperatures (Cosquillo Mejia et al., 2020; Criado et al., 2017; Schaubé et al., 2013; Schmidt et al., 2014), but at the expense of inferior heat transfer rates. On the other hand, if the reaction chamber is separated from the HTF, the reaction pressure can be controlled independently, enabling control of the reaction equilibrium temperature and, in turn, the reaction rate and the heat release/uptake, thereby allowing for stable outflow temperatures during discharging (Ströhle et al., 2017). This allows to form a simple control loop with the HTF outflow temperature and the reactor pressure. The combination of sensible and thermochemical heat storage also addresses the limited operating temperature range of the thermochemical storage alone (Agrafiotis et al., 2016).

In this study, we present the engineering design of a thermochemical reactor for the combined sensible-thermochemical TES system which features several intriguing advantages such as high specific heat storage capacity and low pressure drop, as well as modularity, scalability, and robustness. A lab-scale reactor prototype was fabricated and tested using the CaO/CaCO₃ calcination-carbonation reversible reaction at temperatures around 900°C. The synthesis and characterization of the solid material to avoid sintering and enable cyclic stability is presented. The experimental setup and the performance of the reactor prototype for multiple consecutive cycles are described in detail.

THERMOCHEMICAL REACTOR DESIGN

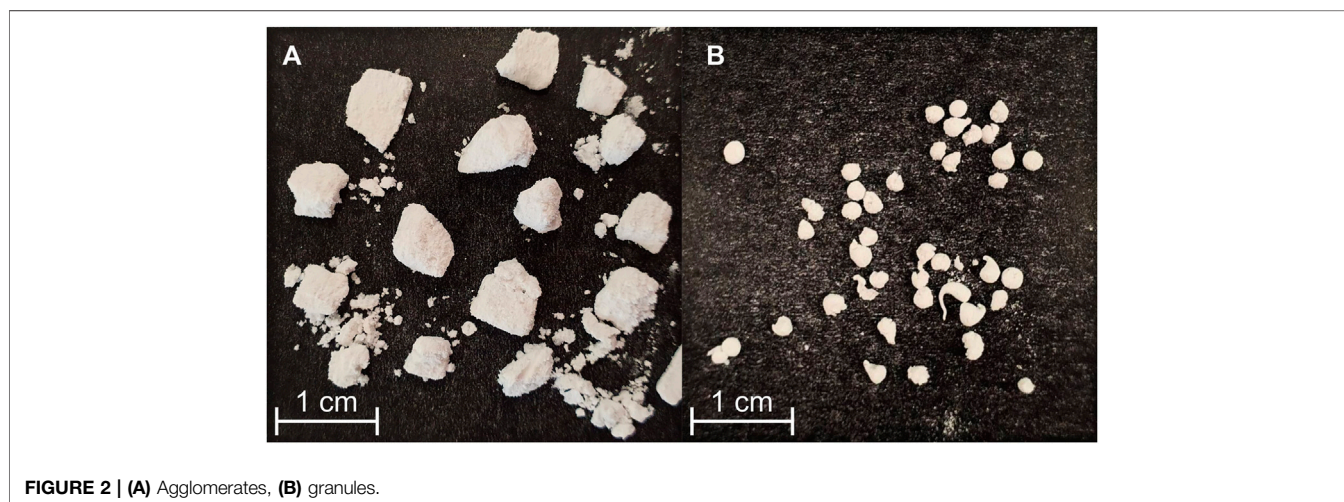
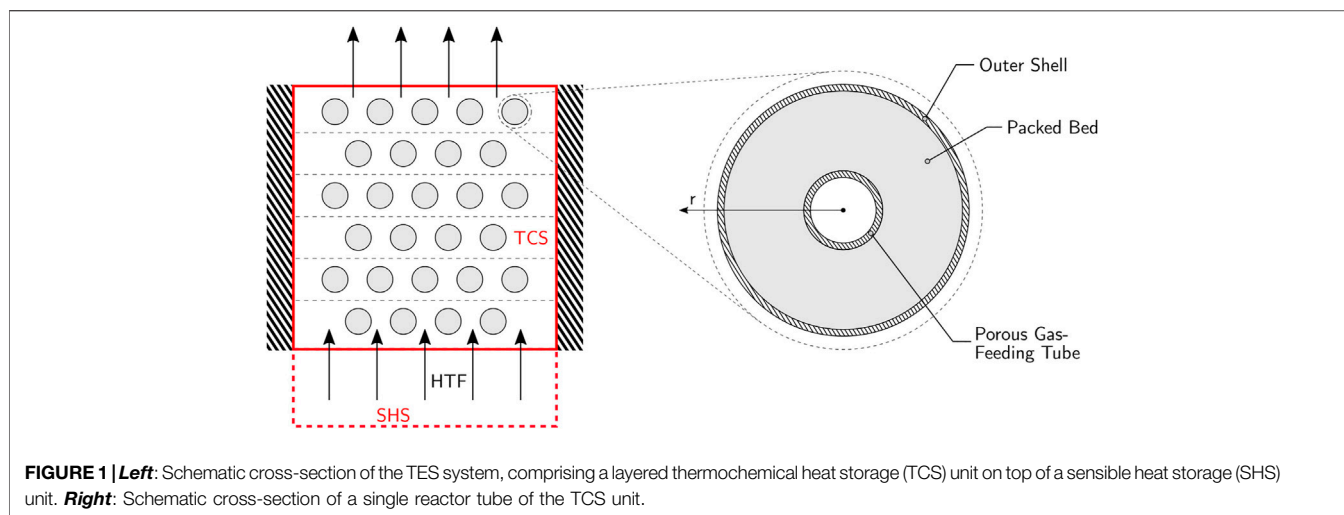
The combined sensible-thermochemical TES system is depicted in **Figure 1A**. It encompasses two units in series: 1) the sensible heat storage (SHS) unit, which consists of a thermocline-based packed bed of rocks or ceramics subjected to the HTF flow; and 2) the thermochemical heat storage (TCS) unit, which consists of a modular array of stacked tubular reactors arranged in a cross-flow heat exchanger configuration. The TCS unit is positioned downstream of the SHS unit and the HTF is common to both. As the SHS unit has already been extensively studied (Hänchen et al., 2011; Zanganeh et al., 2012), the present study focusses on the design and experimental investigation of the TCS unit—i.e., the thermochemical reactor—for performing a reversible endothermic/exothermic gas-solid dissociation reaction of the form $A(s) \leftrightarrow B(s) + C(g)$. Examples are the reduction-oxidation of metal oxides and the calcination-carbonation of metal carbonates (André and Abanades, 2020). In the scope of this investigation, the calcination-carbonation of limestone:



was selected as a model reaction among the various screened metal oxides, hydroxides, sulfides, and carbonates (André et al., 2016), because of its safe handling, reasonably fast reaction rates in both directions, operating temperature in the range 800–1,000°C, and additionally because it is a well-known reaction from the cement manufacturing. **Figure 1B** shows the cross-section of a single reactor tube of the TCS unit. It consists of an outer cylindrical shell, an annular packed bed of solid reactants/products CaO/CaCO₃, and a concentric porous inner tube permeable to the gaseous reactant/product CO₂. This inner tube has a single gas connection on one side for the inlet/outlet of CO₂, which is transported across the porous tube walls to/from the packed bed. With this arrangement, fluid flow is uniform across the packed bed and the pressure drop is kept low. During heat charging, the reactor is partially evacuated to lower the equilibrium temperature, thereby favouring the endothermic calcination of CaCO₃ into CaO, while CO₂ evolved is stored outside the reactor. During discharging, CO₂ is pumped back under higher pressure to the packed bed to increase the equilibrium temperature, thereby favouring the exothermic carbonation of CaO into CaCO₃.

MATERIAL SYNTHESIS AND CHARACTERIZATION

Preliminary experimental runs have indicated poor stability of pure CaCO₃ during multiple carbonation-calcination cycles due to sintering. Thus, MgO obtained by calcination of magnesium oxalate dihydrate (MgC₂O₄·2H₂O) precursor at 700°C was applied as sintering inhibitor (Li et al., 2009). Two synthesis methods with identical final composition were employed: a wet-mixed slurry that is dried to form agglomerates, and a drop granulation method to form granules (Gigantino et al., 2020).



Agglomerates—Magnesium oxide was mixed with calcium acetate ($\text{Ca}(\text{CH}_3\text{COO})_2 \cdot \text{H}_2\text{O}$), adding 2-propanol and left in a roll-mill overnight to mix thoroughly. The slurry was then air-dried and broken into irregular pieces of 4.2 ± 2.3 mm equivalent diameter of a sphere with the same projected surface, as determined by optical granulometry. Calcination at 800°C for 2 h yielded the final material with a composition of $\text{CaO}:\text{MgO} = 58:42\text{wt}$. The synthesized agglomerates have a bulk density of $231 \text{ kg} \cdot \text{m}^{-3}$ when loosely packed and calcined. Variations in sintering temperature (up to 930°C), precursor preparation, particle size, and mixing method were explored to find an optimally stable material formulation. **Figure 2A** shows a sample of the finished agglomerate.

Granules—Magnesium oxide was mixed with sieved ($250 \mu\text{m}$) calcium acetate at a ratio of $\text{MgO}:\text{Ca}(\text{CH}_3\text{COO})_2 \cdot \text{H}_2\text{O} = 1:4.34$ by manual shaking. After adding 6.5%wt pore former ($150 \mu\text{m}$ milled carbon fiber), a binder solution containing ethyl cellulose dissolved in *N*-Methyl-2-pyrrolidone was added to form a slurry. Using a syringe with needle diameter of 1.1 mm, the slurry was

then manually dropped into a stirred beaker containing demineralized water and a surfactant (Tween 80), from a height of around 50 mm. The resulting granules were air-dried before being calcined under atmospheric gas conditions at $1,260^\circ\text{C}$ for 1 h, allowing for the organic components to burn off. The sintered granules have a composition of $\text{CaO}:\text{MgO} = 58:42\text{wt}$ (same as agglomerates), a diameter of 1.74 ± 0.35 mm, and bulk density of $205 \text{ kg} \cdot \text{m}^{-3}$. Pore former contents in the range 0–8.5%wt and sintering temperatures in the range $1,250$ – $1,300^\circ\text{C}$ were also investigated, and the aforementioned values yielded the most stable granules. **Figure 2B** shows a sample of the finished granules.

Performance and cycling stability of both formulations were examined by thermogravimetric analysis (TGA, Netzsch STA 409 CD, flat plate crucible). All TGA experiments were executed with temperature swings between 830°C (carbonation) and 930°C (calcination) under 1 bar CO_2 atmosphere. Plateaus were held for 30 min each, with ramps of $15^\circ\text{C}/\text{min}$ between them. **Figure 3** shows the carbonation extent for 30 consecutive carbonation-

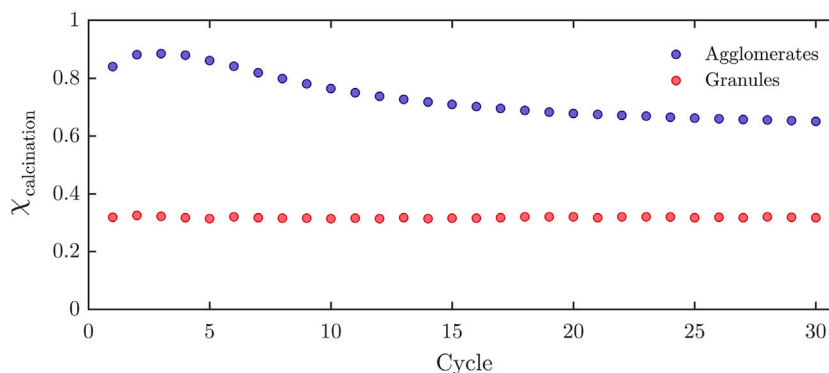


FIGURE 3 | Reaction extents for agglomerates and granules over 30 consecutive carbonation-calcination cycles, performed in the TGA using a temperature-swing between 830°C and 930°C with dwell times of 30 min.

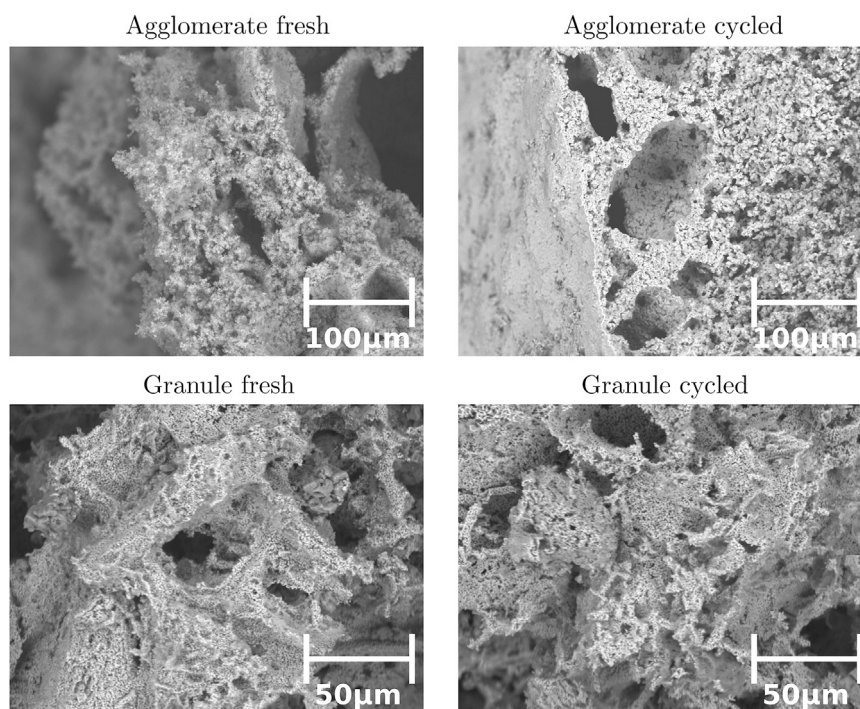


FIGURE 4 | SEM images of agglomerate before (top left) and after cycling (top right), and granules before (bottom left) and after cycling (bottom right).

calcination cycles for both formulations. The reaction extent is defined for each direction as:

$$\chi_{\text{carbonation}} = \frac{n_{\text{CaCO}_3}}{n_{\text{CaCO}_3} + n_{\text{CaO}}}, \quad \chi_{\text{calcination}} = \frac{n_{\text{CaO}}}{n_{\text{CaCO}_3} + n_{\text{CaO}}} \quad (1)$$

For both formulations, the difference between $\chi_{\text{calcination}}$ and $\chi_{\text{carbonation}}$ for any given cycle was less than 1.25%, confirming reversibility. However, agglomerates exhibited an initial $\chi_{\text{carbonation}} = 84.02\%$ which decreased by 22.5% over 30 consecutive cycles. In contrast, the granules exhibited a rather constant reaction extent, initially

$\chi_{\text{carbonation}} = 31.9\%$ which decreased by only 0.49% over 30 consecutive cycles. The degradation in performance of the agglomerates is presumably due to the lower calcination temperature during their synthesis as higher temperatures would break them, which ultimately led to the closing of pores due to sintering during the actual cycling. **Figure 4** shows the SEM images of the agglomerates and granules before and after cycling. It is observed that the boundary of the agglomerate becomes less porous after cycling, while the morphology of the granule remains relatively unchanged.

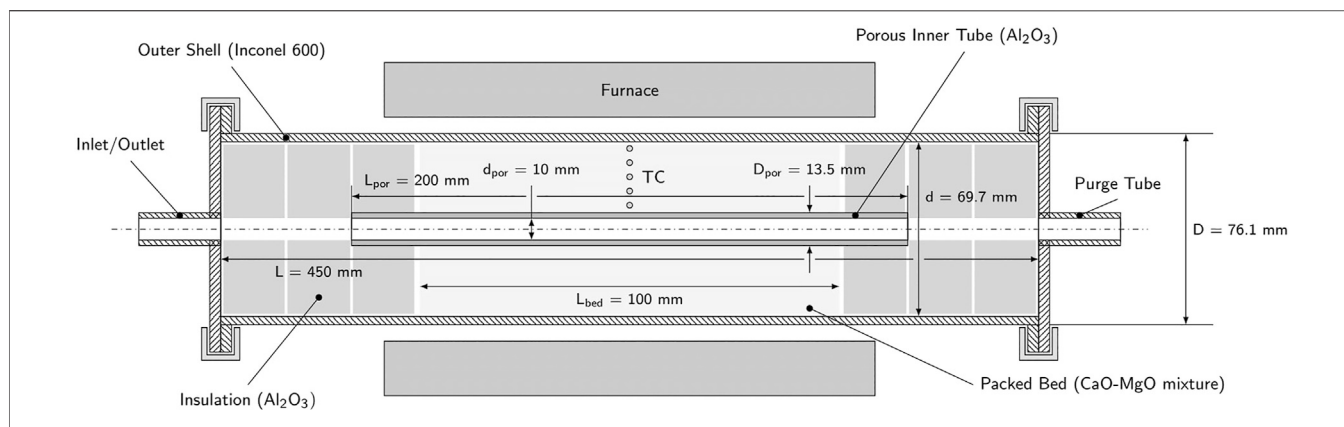


FIGURE 5 | Schematic cross-section of the experimental TCS reactor consisting of an Inconel shell, central porous gas-feeding tube, and annular packed-bed of solid reactants, enclosed by a tubular electric furnace.

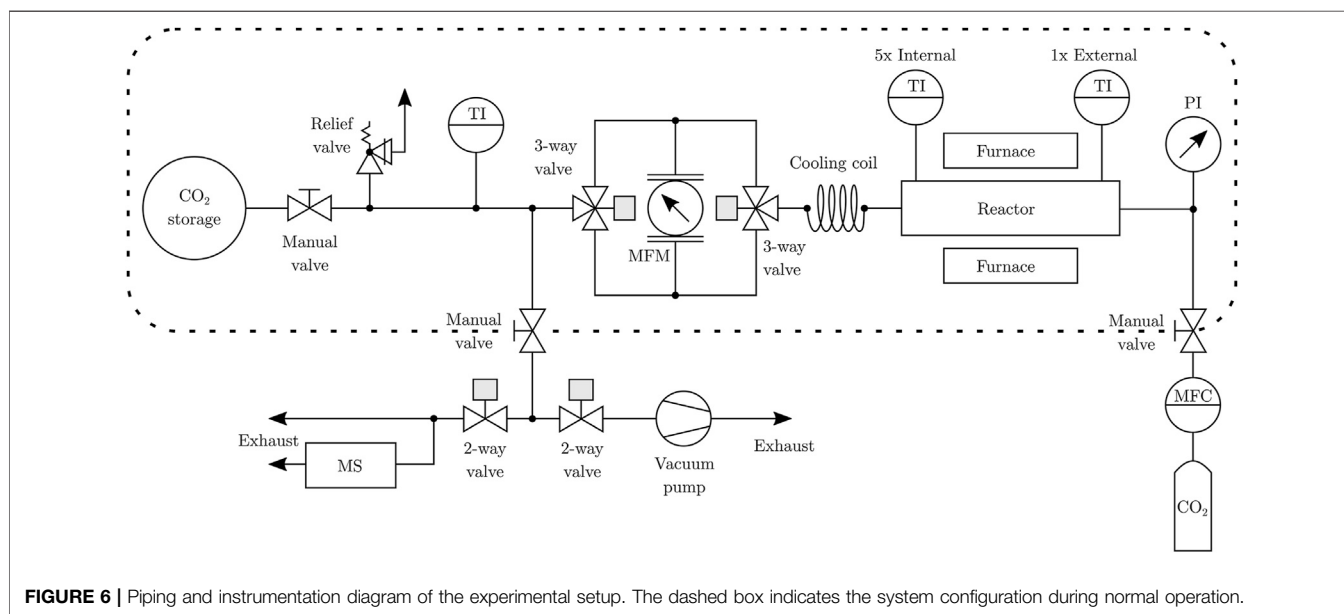


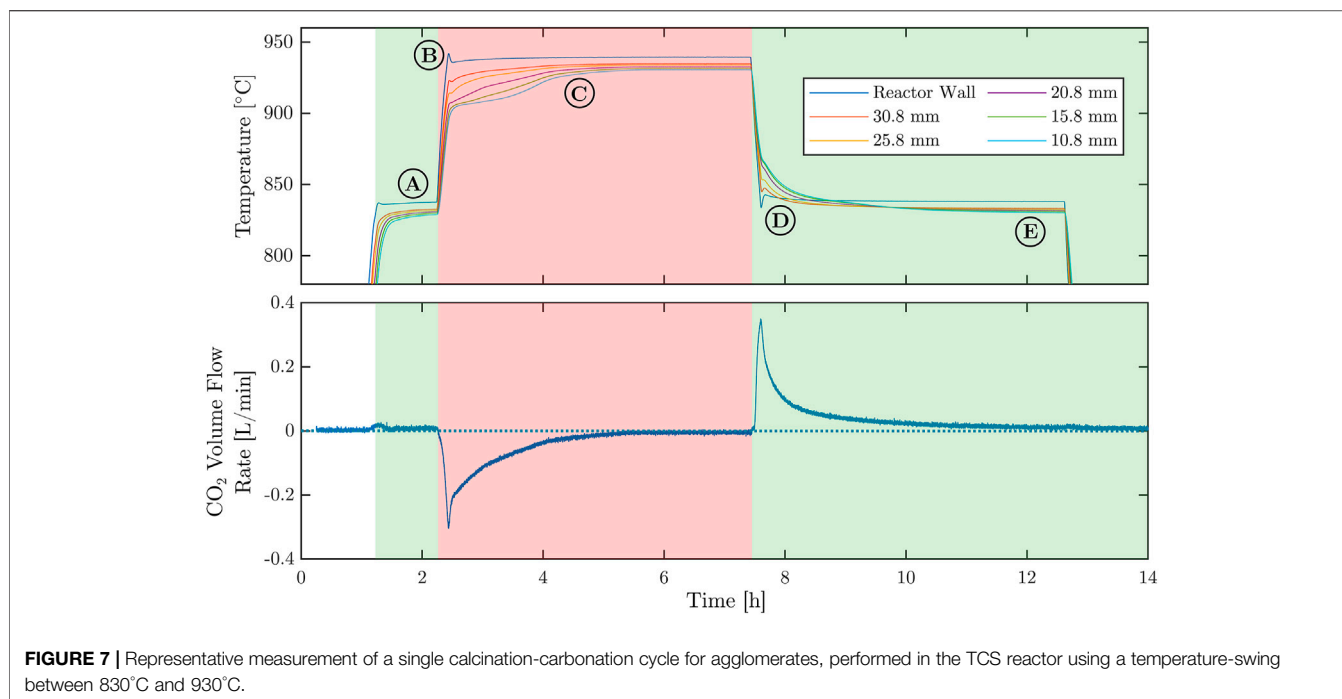
FIGURE 6 | Piping and instrumentation diagram of the experimental setup. The dashed box indicates the system configuration during normal operation.

TCS REACTOR PROTOTYPE AND EXPERIMENTAL SETUP

The lab-scale TCS reactor prototype is schematically shown in **Figure 5**. The main body consists of a 76.1 mm-outer diameter, 3.2 mm-thickness cylindrical shell made of Inconel 600 and a concentric 13.5 mm-outer diameter, 2 mm-thickness porous gas-feeding tube made of alumina (Rauschert Raport P20). These concentric tubes contain the annular packed bed of reactants with an active volume of 364 cm³, enclosed on both sides by Al₂O₃ insulation disks which also hold the central tube in place. Blind flanges fixed with clamps close off the reactor on both sides. Steel tubes are welded concentrically in both flanges, connecting the reactor to the rest of the setup. The reactor is placed in a tubular electric furnace (Carbolite HST 12/200) with a homogeneous

heating zone of 200 mm. Five K-type thermocouples (DIN 60584-2, Cl. 1, ± 1.5°C) are inserted axially to measure the temperature distribution in the packed bed in the radial direction. They are positioned centrally in longitudinal direction and in a horizontal plane at radii of 10.8, 15.8, 20.8, 25.8 and 30.8 mm from the centerline. Two additional shielded thermocouples measure the reactor shell temperature and the outlet gas temperature.

The piping and instrumentation diagram of the complete experimental setup is shown in **Figure 6**. The experimental procedure starts with purging the reactor by vacuum pumping to 100 mbar followed by perfusing with CO₂ from a gas bottle (purity 99.995%). After reaching ambient pressure, the gas bag (Restek gas sampling bag RT-22968) begins to fill. The gas composition is monitored by mass spectrometry (Pfeiffer OmniStar GSD 320 O1). This purging cycle is to verify that



no impurities are left in the system. During normal operation, the manual valves connecting the system to the gas supply and the mass spectrometer/vacuum pump are closed. The furnace then drives the carbonation and calcination cycles. The unidirectional low pressure drop mass flowmeter (Bronkhorst F-201CV, $\pm 1\%$ FS at 4 Ln/min) is embedded in a valve assembly that ensures that the flow is always in the same direction, independent of the current carbonation/calcination state. The LabView control system detects a state change automatically dependent on mass flow and temperature gradient changes, and switches the 3-way valves accordingly.

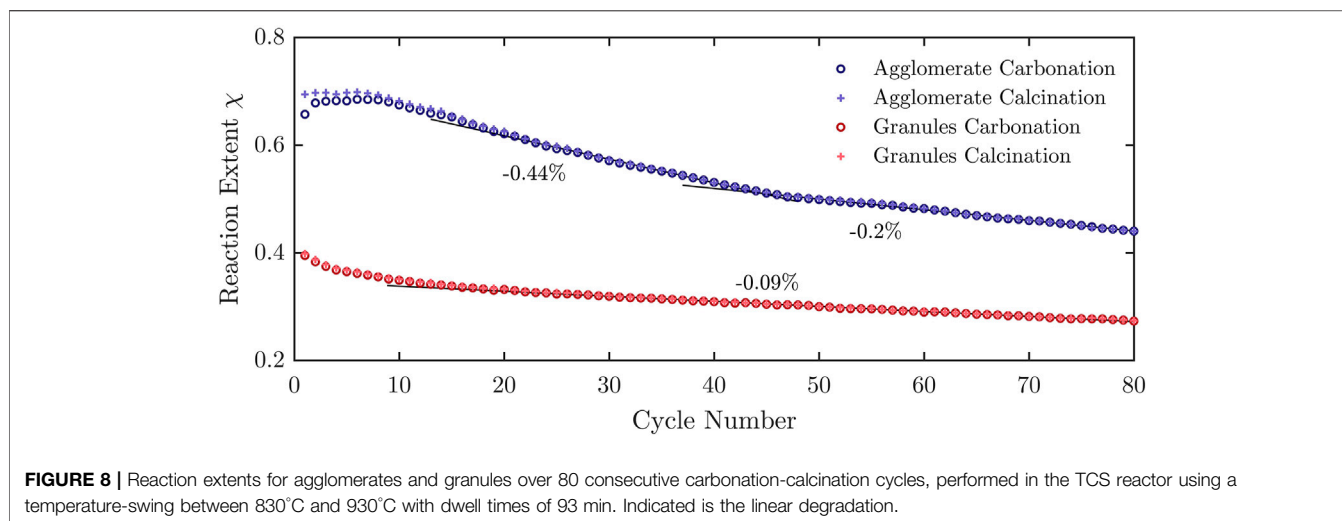
The TCS reactor is operated in a temperature-swing mode under ambient pressure CO_2 . While the use of a gas bag ensures constant ambient pressure, the pressure in the reactor center is constantly monitored to verify that no significant pressure drop is occurring between the two. In this configuration, the only measured input variable is the prescribed temperature profile within the reactor and the only measured output is the CO_2 mass flow rate in/out of the reactor.

EXPERIMENTAL RESULTS WITH THE TCS REACTOR

Single Cycle—After an initial carbonation step held for 1 h, a single calcination/carbonation cycle was conducted with agglomerates using a temperature swing between 835°C and 935°C at a heating/cooling rate of 15°C/min and holding the temperature (plateaus) for 5 h at each reaction step. The duration of this single cycle was much longer than usual (~35 min) for the purpose of studying the temporal variation of temperatures within the packed bed and the corresponding reaction rates as

the reaction extent approaches full completion. **Figure 7** shows the temperatures measured at the reactor wall and within the packed bed (top), and the CO_2 volumetric flow rate (bottom, standard liters per min L/min) as a function of time. Green and red backgrounds indicate the carbonation and calcination steps, respectively. Positive volume flows correspond to CO_2 flow into the reactor during the carbonation step; negative values correspond to the outflow during the calcination step. Five distinct regimes are observed (indicated A–E): A) low volume flow during the first carbonation step because the initial material was mostly already carbonated; B) slight temperature overshoot because of the set point controller of the tubular furnace; C) temperature profiles change because of the endothermic calcination step and approach steady-state as the calcination reaches completion; D) same effect as for regime C but for the subsequent exothermic carbonation; and E) noticeable temperature drop from the reactor wall to the packed bed at approximate steady-state conditions because of heat losses by conduction.

Reactor modelling indicates that the reaction extent is locally approaching chemical equilibrium, such that mass and heat transfer effects are dominating (Wild and Steinfeld, 2021). The relatively slow reaction rates observed are mainly attributed to the poor heat transfer rate of the packed bed, which is predominantly driven by conduction across the porous medium. This rate-controlling mechanism is strongly dependent on the effective thermal conductivity of the packed bed, which in turn depends on the morphology of the solid reactants, and can impose an upper size limitation on the radial thickness of the annular packed bed. As aforementioned, the upscaling foresees the use of an array of tubular reactors, each containing an annular packed bed with radial thickness of comparable magnitude as the one of the prototype reactor.



Multiple Cycles—Experimental runs with 80 consecutive carbonation/calcination cycles were conducted for both agglomerates and granules using a temperature swing between 830°C and 930°C with a duration of 93 min for each step. Since shrinking had been observed with the fresh synthesized material, the reactants were cycled for over 80 cycles beforehand. A mass of 133.17 g of agglomerate, and 102.72 g of granules were loaded into the reactor. The theoretical maximum CO₂ volume corresponds to 23.23 and 17.92 L (standard liters), respectively. Gas volumes were used to determine the reaction extent.

Figure 8 shows the measured carbonation and calcination reaction extents for both formulations. Similar to the TG runs, the mean difference between $\chi_{\text{calcination}}$ and $\chi_{\text{carbonation}}$ was 0.57% for agglomerates and 0.41% for granules, confirming reversibility. However, for the agglomerates, a linear degradation by about 0.44% per cycle is observed from cycle #15 to #45 and by 0.2% per cycle from cycle #45 to #80. The reaction extent decreased from a maximum $\chi_{\text{calcination}} = 68.5\%$ for cycle #6, corresponding to a measured uptake/release CO₂ volume of 15.91 L, to a minimum $\chi_{\text{calcination}} = 44.1\%$ for cycle #80, corresponding to 10.27 L CO₂. Clearly, the granules exhibited superior cyclic stability but still some degradation by about 0.09% per cycle, from the initial maximum $\chi_{\text{calcination}} = 39.5\%$ for cycle #1, corresponding to 7.08 L CO₂, to $\chi_{\text{calcination}} = 27.4\%$ for cycle #80, corresponding to 4.92 L CO₂. Thus, over 80 consecutive cycles, the degradation observed was 35.4% for agglomerates and 30.4% for granules.

Based on the maximal CO₂ volumes measured, the calculated specific gravimetric and volumetric heat storage capacities were 866 kJ/kg and 322 MJ/m³ for agglomerates, respectively, and 450 kJ/kg and 134 MJ/m³ for granules, respectively. The higher energy densities of the agglomerates (both volumetric and gravimetric) came at the cost of poor stability over consecutive cycles. The granules exhibited very good cycling stability over 30 consecutive cycles in the TGA, but degradation was observed over 80 consecutive cycles in the reactor. This is attributed primarily to heat and mass transfer effects in the packed bed reactor vis-a-vis a single layer of granules and shorter cycle duration in the TGA. These

detrimental effects could be mitigated under pressure-swing isothermal operation.

An upper limit to the pressure drop in radial direction across the packed bed was calculated based on Darcy's law using values of permeability $\kappa = 4.086 \cdot 10^{-13} \text{ m}^2$ and $\kappa_l = 5.675 \cdot 10^{-8} \text{ kg} \cdot \text{Pa}^{-1} \cdot \text{s}^{-2}$ determined in a separate experiment. Assuming radial velocity of 0.0017 m/s at the inner boundary of the packed bed (corresponding to the highest measured values of the mass flow rate at 0.42 L/min), the maximum pressure drop for agglomerates over the complete bed is 31 mbar, confirming the low pressure drop for this radial flow configuration of the TCS reactor.

SUMMARY AND CONCLUSION

We have designed a thermochemical reactor for the storage of high-temperature process heat using a reversible reaction of the form $A(s) \leftrightarrow B(s) + C(g)$ which can be particularly applied to metal oxides, hydroxides, sulfides, and carbonates. The CaO carbonation - CaCO₃ calcination reaction was selected as model reaction. To prevent sintering CaO:MgO = 58:42wt was synthesized in the form of agglomerates and granules. As proof-of-concept, we have fabricated a lab-scale single-tube reactor prototype and demonstrated its operation for 80 consecutive cycles in a 830–930°C temperature-swing mode. The cyclic stability for granules was clearly superior than that for agglomerates. The experimental data obtained has been used to validate a heat and mass transfer numerical model for design optimization (Wild and Steinfeld, 2021). The TCS reactor is modular and scalable in a cross-flow heat exchanger configuration, can be operated in both temperature-swing and pressure-swing cyclic modes, and can be combined in series with a thermocline-based sensible heat storage. When applied to store concentrated solar heat, it enables the decarbonization of several key energy-intensive industrial processes such as metallurgical processing and cement manufacturing, as well as the efficient thermal production of solar power and fuels.

DATA AVAILABILITY STATEMENT

The raw data supporting the conclusion of this article will be made available by the authors, without undue reservation.

AUTHOR CONTRIBUTIONS

MW and AS conceived the process and associated thermochemical reactor; MW and LL synthesized the materials, executed the experiments, and processed the experimental data; AS supervised the project; all authors contributed to the writing of the manuscript.

REFERENCES

- Abedin, A. H., and Rosen, M. A. (2011). A Critical Review of Thermochemical Energy Storage Systems. *Torej* 4, 42–46. doi:10.2174/1876387101004010042
- Agrafiotis, C., Roeb, M., and Sattler, C. (2016). Exploitation of Thermochemical Cycles Based on Solid Oxide Redox Systems for Thermochemical Storage of Solar Heat. Part 4: Screening of Oxides for Use in Cascaded Thermochemical Storage Concepts. *Solar Energy* 139, 695–710. doi:10.1016/j.solener.2016.04.034
- André, L., Abanades, S., and Flamant, G. (2016). Screening of Thermochemical Systems Based on Solid-Gas Reversible Reactions for High Temperature Solar thermal Energy Storage. *Renew. Sust. Energ. Rev.* 64, 703–715. doi:10.1016/j.rser.2016.06.043
- André, L., and Abanades, S. (2020). Recent Advances in Thermochemical Energy Storage via Solid-Gas Reversible Reactions at High Temperature. *Energies* 13, 5859. doi:10.3390/en13225859
- Carrillo, A. J., González-Aguilar, J., Romero, M., Coronado, J. M., González-Aguilar, J., Romero, M., et al. (2019). Solar Energy on Demand: A Review on High Temperature Thermochemical Heat Storage Systems and Materials. *Chem. Rev.* 119, 4777–4816. doi:10.1021/acs.chemrev.8b00315
- Cosquillo Mejia, A., Afflerbach, S., Linder, M., and Schmidt, M. (2020). Experimental Analysis of Encapsulated CaO/Ca(OH)₂ Granules as Thermochemical Storage in a Novel Moving Bed Reactor. *Appl. Therm. Eng.* 169, 114961. doi:10.1016/j.applthermaleng.2020.114961
- Criado, Y. A., Huille, A., Rougé, S., and Abanades, J. C. (2017). Experimental Investigation and Model Validation of a CaO/Ca(OH)₂ Fluidized Bed Reactor for Thermochemical Energy Storage Applications. *Chem. Eng. J.* 313, 1194–1205. doi:10.1016/j.cej.2016.11.010
- Geissbühler, L., Mathur, A., Mularczyk, A., and Haselbacher, A. (2019). An Assessment of Thermocline-Control Methods for Packed-Bed thermal-energy Storage in CSP Plants, Part 1: Method Descriptions. *Solar Energy* 178, 341–350. doi:10.1016/j.solener.2018.12.015
- Gigantino, M., Sas Brunser, S., and Steinfeld, A. (2020). High-Temperature Thermochemical Heat Storage via the CuO/Cu₂O Redox Cycle: From Material Synthesis to Packed-Bed Reactor Engineering and Cyclic Operation. *Energy Fuels* 34, 16772–16782. doi:10.1021/acs.energyfuels.0c02572
- Glatzmaier, G. (2011). *Summary Report for Concentrating Solar Power Thermal Storage Workshop: New Concepts and Materials for Thermal Energy Storage and Heat-Transfer Fluids*, 2011.
- Hänchen, M., Brückner, S., and Steinfeld, A. (2011). High-temperature thermal Storage Using a Packed Bed of Rocks - Heat Transfer Analysis and Experimental Validation. *Appl. Therm. Eng.* 31, 1798–1806. doi:10.1016/j.applthermaleng.2010.10.034
- Henry, A., Prasher, R., and Majumdar, A. (2020). Five thermal Energy Grand Challenges for Decarbonization. *Nat. Energ.* 5, 635–637. doi:10.1038/s41560-020-0675-9
- King, K., Randhir, K., Petrasch, J., and Klausner, J. (2019). Enhancing Thermochemical Energy Storage Density of Magnesium-manganese Oxides. *Energy Storage* 1. doi:10.1002/est.2.83
- Kuravi, S., Trahan, J., Goswami, D. Y., Rahman, M. M., and Stefanakos, E. K. (2013). Thermal Energy Storage Technologies and Systems for Concentrating

FUNDING

We gratefully acknowledge the financial support by the Swiss National Science Foundation (Project No. 173438).

ACKNOWLEDGMENTS

We thank Philipp Haueter, Marco Gigantino, Brendan Bulfin, Thomas Frei, Simon Meier, Paul Leudet de Vallée, and Julian Urech for the technical support with the material synthesis, experimental setup and experimental campaign.

- Solar Power Plants. *Prog. Energ. Combustion Sci.* 39, 285–319. doi:10.1016/j.pecc.2013.02.001
- Li, L., King, D. L., Nie, Z., and Howard, C. (2009). Magnesia-Stabilized Calcium Oxide Absorbents with Improved Durability for High Temperature CO₂ Capture. *Ind. Eng. Chem. Res.* 48, 10604–10613. doi:10.1021/ie901166b
- Mette, B., Kerskes, H., and Drück, H. (2012). Concepts of Long-Term Thermochemical Energy Storage for Solar thermal Applications - Selected Examples. *Energ. Proced.* 30, 321–330. doi:10.1016/j.egypro.2012.11.038
- Mostafavi Tehrani, S. S., Taylor, R. A., Nithyanandam, K., and Shafiei Ghazani, A. (2017). Annual Comparative Performance and Cost Analysis of High Temperature, Sensible thermal Energy Storage Systems Integrated with a Concentrated Solar Power Plant. *Solar Energy* 153, 153–172. doi:10.1016/j.solener.2017.05.044
- Neises, M., Tescari, S., de Oliveira, L., Roeb, M., Sattler, C., and Wong, B. (2012). Solar-heated Rotary kiln for Thermochemical Energy Storage. *Solar Energy* 86, 3040–3048. doi:10.1016/j.solener.2012.07.012
- Peng, X., Root, T. W., and Maravelias, C. T. (2017). Storing Solar Energy with Chemistry: the Role of Thermochemical Storage in Concentrating Solar Power. *Green. Chem.* 19, 2427–2438. doi:10.1039/c7gc00023e
- Roos, P., and Haselbacher, A. (2021). Thermocline Control through Multi-Tank thermal-energy Storage Systems. *Appl. Energ.* 281, 115971. doi:10.1016/j.apenergy.2020.115971
- Schaube, F., Kohzer, A., Schütz, J., Wörner, A., and Müller-Steinhagen, H. (2013). De- and Rehydration of Ca(OH)₂ in a Reactor with Direct Heat Transfer for Thermo-Chemical Heat Storage. Part A: Experimental Results. *Chem. Eng. Res. Des.* 91, 856–864. doi:10.1016/j.cherd.2012.09.020
- Schmidt, M., Szczukowski, C., Roßkopf, C., Linder, M., and Wörner, A. (2014). Experimental Results of a 10 kW High Temperature Thermochemical Storage Reactor Based on Calcium Hydroxide. *Appl. Therm. Eng.* 62, 553–559. doi:10.1016/j.applthermaleng.2013.09.020
- Schrader, A. J., Schieber, G. L., Ambrosini, A., and Loutzenhiser, P. G. (2020). Experimental Demonstration of a 5 kWth Granular-Flow Reactor for Solar Thermochemical Energy Storage with Aluminum-Doped Calcium Manganite Particles. *Appl. Therm. Eng.* 173, 115257. doi:10.1016/j.applthermaleng.2020.115257
- Stekli, J., Irwin, L., and Pitchumani, R. (2013). Technical Challenges and Opportunities for Concentrating Solar Power with Thermal Energy Storage. *Therm. Sci. Eng. Appl.* 5, 021011. doi:10.1115/1.4024143
- Ströhle, S., Haselbacher, A., Jovanovic, Z. R., and Steinfeld, A. (2017). Upgrading Sensible-Heat Storage with a Thermochemical Storage Section Operated at Variable Pressure: An Effective Way toward Active Control of the Heat-Transfer Fluid Outflow Temperature. *Appl. Energ.* 196, 51–61. doi:10.1016/j.apenergy.2017.03.125
- Wild, M., and Steinfeld, A. (2021). A Thermochemical Energy Storage Reactor Model - Code Formulation, Verification, and Experimental Validation. In Proceedings of the CHT-21 International Symposium on Advances in Computational Heat Transfer. Rio de Janeiro, Brazil, Aug. 15–19.
- Yuan, Y., Li, Y., and Zhao, J. (2018). Development on Thermochemical Energy Storage Based on CaO-Based Materials: A Review. *Sustainability* 10, 2660. doi:10.3390/su10082660

- Zanganeh, G., Khanna, R., Walser, C., Pedretti, A., Haselbacher, A., and Steinfeld, A. (2015). Experimental and Numerical Investigation of Combined Sensible-Latent Heat for thermal Energy Storage at 575°C and above. *Solar Energy* 114, 77–90. doi:10.1016/j.solener.2015.01.022
- Zanganeh, G., Pedretti, A., Zavattoni, S., Barbato, M., and Steinfeld, A. (2012). Packed-bed thermal Storage for Concentrated Solar Power - Pilot-Scale Demonstration and Industrial-Scale Design. *Solar Energy* 86, 3084–3098. doi:10.1016/j.solener.2012.07.019

Conflict of Interest: The authors declare that the research was conducted in the absence of any commercial or financial relationships that could be construed as a potential conflict of interest.

Publisher's Note: All claims expressed in this article are solely those of the authors and do not necessarily represent those of their affiliated organizations, or those of the publisher, the editors and the reviewers. Any product that may be evaluated in this article, or claim that may be made by its manufacturer, is not guaranteed or endorsed by the publisher.

Copyright © 2021 Wild, Lüönd and Steinfeld. This is an open-access article distributed under the terms of the Creative Commons Attribution License (CC BY). The use, distribution or reproduction in other forums is permitted, provided the original author(s) and the copyright owner(s) are credited and that the original publication in this journal is cited, in accordance with accepted academic practice. No use, distribution or reproduction is permitted which does not comply with these terms.